Title

Three-dimensional fracture continuum characterization aided by surface time-domain electromagnetics and hydrogeophysical joint inversion—proof-of-concept

Journal

Computational Geosciences, 24(5)

ISSN

1420-0597

Authors

Commer, Michael
Finsterle, Stefan
Hoversten, G Michael

Publication Date

2020-10-01

DOI

10.1007/s10596-020-09942-9

Peer reviewed

Computational geosciences manuscript No.
(will be inserted by the editor)

Three-dimensional fracture continuum characterization aided by surface time-domain electromagnetics and hydrogeophysical joint inversion - proof-of-concept

Michael Commer · Stefan Finsterle · G. Michael Hoversten

Received: June 23, 2020/ Accepted:

Abstract Efficient and safe production of hydraulically fractured reservoirs benefits from the prediction of their geometrical attributes. Geophysical methods have the potential to provide data that is sensitive to fracture geometries, alleviating the typically sparse nature of in situ reservoir observations. Moreover, surface-based methods can be logistically and economically attractive since they avoid operational interference with the injection-well infrastructure. This contribution investigates the potential of the surface-based time-domain electromagnetic (EM) method. EM methods can play an important role owing to their sensitivity to injection-induced fluid property changes. Two other advantageous factors are the EM signal-enhancing effect of vertical steel-cased wells and the fact that injected proppants can be enhanced to produce a stronger electrical conductivity contrast with the reservoir's connate fluid. Nevertheless, an optimal fracture characterization will no doubt require the integration of EM and reservoir injection and production data. We hence carry out our investigations within a hydrogeophysical parameter estimation framework where EM data and injection flow-rates are combined in a fully coupled way. Given the interdisciplinary nature of coupled hydrogeophysical inverse modeling, we dedicate one section to laying out key aspects in a didactic manner.

Keywords Fracture parameter estimation · Coupled hydrogeophysical inverse modeling · Time-domain electromagnetics · Petrophysical transformation · Parameter correlation

M. Commer
Lawrence Berkeley National Laboratory, Earth and Environmental Sciences Area, Berkeley, California, USA
Tel: +1-510-4866164, Fax: +1-510-4865686, E-mail: MCommer@lbl.gov

S. Finsterle
Finsterle GeoConsulting, Kensington, California, USA

G. Michael Hoversten
Chevron Energy Technology Company, Houston, Texas, USA

1 Introduction

With the onset of high production from land-based unconventional hydrocarbon reservoirs, the characterization of hydraulically fractured zones has become an important factor for production optimization. Efficient production requires prediction of the extent, orientation, and active surface area of fractures or fracture networks that are created and/or activated. Remotely sensing geophysical methods promise to provide a relatively inexpensive set of tools for deriving fracture attributes [16,29], given their generally larger spatial coverage compared to well data. Two classes of geophysical methods, seismic and electromagnetic, are sensitive to the hydromechanical property changes accompanying fracture evolution as well as hydraulic state changes in existing fractures.

Using active (artificially sourced) seismic methods, one can utilize the fracture-induced occurrence of anisotropy in P-wave attenuation [12] and the scattering of seismic waves [18]. Passive seismic methods sense microearthquake (MEQ) activity when injected fluids create new fractures or reactivate existing ones, thus providing reservoir feedback in terms of the evolution of fracture permeability [35].

MEQ surveys have become critical input to simulations involving discrete fracture models (DFM). Coupled geomechanical modeling [51] and flow simulation in MEQ-derived DFMs are used to predict stimulated reservoir volume (SRV). SRV estimates are critical for optimal well placement; however, they can be uncertain due to the following reasons. First, MEQ event locations strongly depend on the (seismic) velocity model used. Moreover, SRV estimates can change dramatically when velocity models are updated. Even when MEQ event locations are accurate, by themselves MEQ events cannot tell if an injected proppant has reached the MEQ locations or if fractures associated with MEQ events are connected to the well bore. Additionally, a proppant reaching existing fractures does not guarantee measureable MEQ events. Proppants are solid materials designed to prevent the closing of induced fractures [34].

Electromagnetic (EM) methods have proven their potential for remote fracture characterization [2,32]. Further, they can alleviate some of the aforementioned shortcomings, while being an economic alternative to seismic methods, mainly due to their strong sensitivity to property changes caused by fluid substitution [25,38,49]. Additives to proppants can further enhance the sensitivity by boosting an injectate's electrical properties, thus magnifying reservoir changes [24].

EM geophysical systems can roughly be divided between borehole tools and non-borehole tools. Borehole source and receiver tools operate inside wells and are thus limited in terms of power and source-receiver separations. This translates into limited depth of investigation away from the borehole. Surface EM systems make use of the same physics as borehole tools. However, they enable both higher source moments and larger source-receiver separations, thus allowing for larger depths of investigation [43]. For example, numerical sensitivity studies have indicated that conventional surface EM exploration systems can detect fractures at a depth of 3 km [28].

Generally, all EM methods suffer from a loss of spatial resolution with increasing depth of investigation. Compared to seismic systems, the resolution loss with distance occurs at a higher rate, because the energy loss due to propagation is much higher. For surface EM source configurations, the spatial resolution loss with depth can be mitigated by exploiting the metallic electrical conductivity of vertical steel-cased boreholes. By placing the current-injecting source electrodes in the vicinity of steel-cased boreholes, the highly conductive casing can act as a vertical antenna with an extended source dipole moment, thus providing an enhanced electrical connection to the reservoir. This can amplify EM responses due to subtle reservoir property changes and hence make them measurable at the surface. Three-dimensional (3D) numerical verifications of this concept have focused on hydraulic fracture monitoring [28, 15].

The present work is a proof-of-concept for the characterization of deep fracture zones by using joint inverse modeling of EM and hydrological data. We consider a scenario modeled after an undisclosed field case, where the injection point is located at a depth of 2145 m below ground surface. The case involves the time-domain EM (TEM) method [36] used in a configuration where both transmitter and receivers are at the surface. In comparison to in situ measurements, the surface setup can be economically advantageous by avoiding a potential interference with injection well infrastructure during operation.

Fusing hydrological with geophysical methods is a rapidly evolving discipline, e.g. [44,46,47]; within, hydrogeophysical fracture characterization is currently at an even more infant state due to the involved complexities. Geophysical data types that have been employed for this purpose are crosshole seismic traveltimes [11], seismic scattered wavefield data [30], and ground-penetrating radar [6,17,41]. This work advances hydrogeophysical fracture characterization by exploring the TEM method. While the TEM method has proven its monitoring potential for fracture applications [28,50], to the best of our knowledge, it has not yet been part of inverse-modeling for fracture identification.

We also incorporate recent findings about the steel-casing effect [45] into the 3D TEM-data simulation module. Our overarching coupled hydrogeophysical inversion scheme estimates hydraulic permeability and geometry parameters of a stimulated fracture zone in a 3D parametric manner, where a steel-casing approximation is part of an electrical conductivity background model. Injection flow-rate data and TEM data are inverted separately and jointly in order to demonstrate the improved geometrical resolution.

Given the interdisciplinary nature of this type of hydrogeophysical joint inversion application, we dedicate Section 2.4 to exposing essential aspects in an explanatory way.

2 Methodology: Hydrogeophysical inversion for estimating fracture parameters

Enhanced production from hydraulically fractured reservoirs requires the appraisal of bulk geometrical and hydraulic fracture properties in order to obtain SRV estimates. However, most realistic scenarios involve geometrically fine and complex fracture networks with spatial scales below the minimum resolvable scales that result from the spatial resolution loss of remotely-sensing EM methods. We thus represent stimulated fractures and associated networks of secondary, small fractures as a continuum with a hydraulic permeability that is distinct from the background. The main stimulated fracture and associated secondary fracture network are thereby conceptualized as a single continuum that occupies a geometrically discrete zone. For example, Fig. 1 illustrates the parametric representation of a 3D ellipsoidal fracture continuum, described by the following parameters:

1. Background hydraulic permeability (k_b)
2. Fracture continuum hydraulic permeability (k_f)
3. Spatial fracture continuum extension in x (D_x)
4. Spatial fracture continuum extension in y (D_y)
5. Spatial fracture continuum extension in z (D_z)
6. Azimuth angle

The ellipsoid's center coincides with the fluid injection point used for both hydraulic fracturing and post-fracturing characterization. The injection point is connected to the surface through a vertical steel casing of length 2145 m.

To provide enough of an EM signal difference with respect to the pre-injection state, a large enough electrical conductivity contrast needs to exist between the injection zone and the rest of the formation. Recent research has focused on contrast agents, i.e. additive substances that increase the electrical properties of injected fluids with respect to the connate fluids of the surrounding formation, e.g. [37]. We simulate the injection of such a conductively enhanced fluid taking place over a 70-minutes period, where the flow rate is measured at the injection point. A total of 50 samples are distributed over the injection period, representing our hydrological data set that is to be complemented by a geophysical (TEM) data set.

2.1 Simplifying assumptions

Our proof-of-concept involves both geometrical and conceptual simplifications. First, the fracture zone represented by a continuum has an ellipsoidal shape approximating a vertical, sheet-like structure. One of its horizontal extensions, here chosen to be D_y, is set as known and relatively small compared to the other axes. Table 1 (column "True value") lists the 6 actual values of the forward-modeling input parameters.

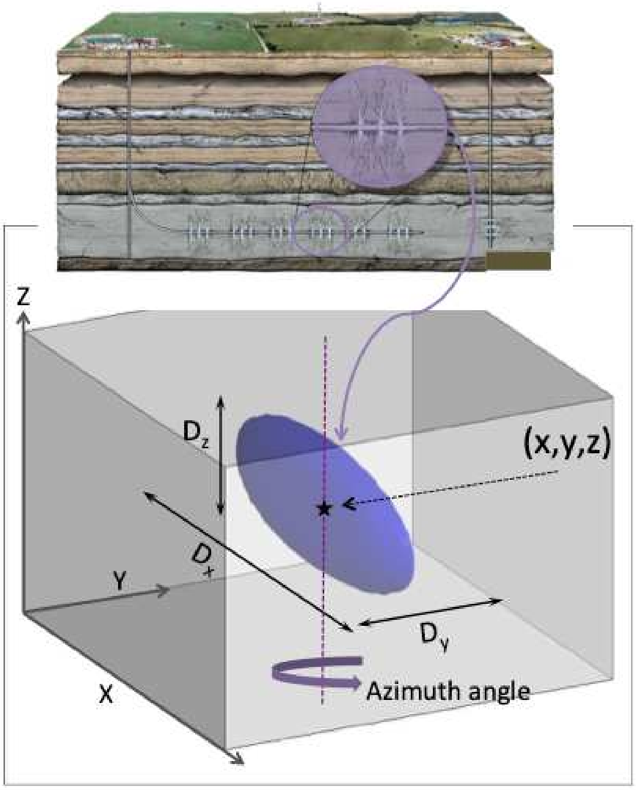

Fig. 1 Illustration of the representation of a fracture network by an ellipsoidal region in a Cartesian coordinate system. The ellipsoid mimics a fracture continuum described by size parameters (D_x, D_y, D_z) and one rotational degree of freedom given by an azimuth angle. The parameterization does not consider a vertical inclination. The center point is fixed in the inversion and coincides with the injection point.

Table 1 Parameter bounds, actual values, initial guesses, and estimates. Permeability values k are given in milliDarcy (mD, 1 mD $\approx 10^{-15}$ m^2) and the SI unit m^2 where a logarithmic transform is used in the inversion. The model parameter Y-extent (D_y) is kept fixed during the inversion. Stimulated reservoir volumes (SRV) are calculated from the size parameters D_x,D_y,D_z for an ellipsoidal shape.

Parameter type		Lower bound	Upper bound	True value	Starting guess	Estimated: Flow-rate inversion	Estimated: Joint inversion
Permeability k of rock matrix	(mD)	0.1	10,000	1	10	4	0.964
	$\log_{10}(k)$ (m^2)	-16	-11	-15	-14	-14.398	-15.016
Permeability k of frac. cont.	(mD)	10	10^7	1,000	30,200	991	992
	$\log_{10}(k)$ (m^2)	-14	-8	-12	-10.523	-12.004	-12.003
X-extent D_x (m)		50	700	250	400	119.69	254.37
Y-extent D_y (m)		-	-	20	-	-	-
Z-extent D_z (m)		50	700	90	150	113.76	89.86
Azimuth (deg)		N/A	N/A	0	20	172.27	0.27
Estimated SRV (10^6m^3)		0.0262	5.1313	0.2356	0.6283	0.1426	0.2394

The geometrical simplification is based on research that the evolution of single, wide, and sheet-like fractures can be favored by oriented well perforations [1]. Such casing perforations would be required to be aligned in the direction that the formation is most likely to fracture when applying hydraulic pressure. On the other hand, it has been argued that despite the usage of oriented perforations, other factors such as formation heterogeneity and/or formation dip can still lead to less predictable and geometrically more complicated fractures, e.g., [22]. While our model includes no background formation heterogeneity, we still allow for some additional complexity by means of a rotational degree of freedom. As shown in Fig. 1, this is given by the azimuth angle with respect to the z-axis which coincides with the vertical borehole.

The second geometrical simplification ignores the presence of horizontal well sections, that is, the fracture zone is assumed to be at the bottom of the vertical well. Furthermore, the assumption of a homogeneous and isotropic background holds for both the hydraulic and geophysical properties. The background permeability is constant at 1 mD (milliDarcy), or 10^{-15} m^2, and the electrical conductivity is constant at σ=10^{-2} S/m, which is equivalent to a resistivity of ϱ=100 Ωm. Note that this article uses both conductivity and its inverse, resistivity.

Our conceptual model simplification involves the exclusion of porosity parameters in the inverse modeling, thus assuming a fixed storativity of the fracture and non-fractured aquifer. The evolution of the flow rate over time depends on the hydraulic diffusivity, which is the ratio of hydraulic conductivity and storativity. While these two quantities cannot be identified independently from single-hole data, their ratio can. Hence, we opt to adjust only permeability, while storativity is fixed. The late-time flow evolution also depends on the properties of the non-fractured aquifer. However, since the non-fractured portion has a much lower hydraulic diffusivity compared to the fracture, its parameters cannot be identified during the high-flow-rate portion of the test, because leak-off into the matrix is very minor compared to the total flow rate. Leak-off could potentially be estimated from the long tail of the flow rate data, however this is not the objective of our analysis.

The electromagnetic properties of our model involve two simplifications. The first ignores directionally dependent electrical conductivity, i.e. anisotropy. Owing to the heterogeneity of fractured pore space, as illustrated by the upper Fig. 1, preferential fluid flow can cause preferential current flow and thus an anisotropy effect. Thin alternating sequences of resistive and conductive sediments, can, for example, cause the same kind of anisotropy [42,31]. Our approxmiation by a thin ellipsoid may account for this to some degree. A more flexible way involves an appropriate bulk anisotropy coefficient [3], representing another inversion parameter, which we omit here for our goal of a simple proof-of-concept. A separate coefficient can be introduced to handle anisotropy of the formation away from the fracture.

Note that effects due to electrical anisotropy are distinct from the casing effect. The latter causes vertical current-channeling and horizontal current leak-off due to the casing's metallic conductivity. Our simulations approximate these effects as will be detailed below.

Finally, we assume the absence of polarizable and ferromagnetic materials by assigning the permittivity and magnetic permeability of vacuum to both the fracture zone and the surrounding media. Induced polarization effects can play a role in fracture imaging, for example when rocks exhibit dispersivity [8], and, especially, when injected proppants are engineered to exhibit capacitive behaviour [7,4].

2.2 Hydrogeophysical inverse-modeling framework

Inverse modeling enables us to explore and compare the informational content of the two data types considered here. These are total fluid flow rates measured at the injection point and time-domain electric fields excited and recorded at the surface. The merging of these two different data types in an inverse-modeling scheme involves a multiphysics forward modeling scheme, where the primary forward modeling operator simulates all processes related to the flow of injected fluid. It is given by the flow and transport simulator TOUGH2 [39], which has modeling capabilities for multiphase, multicomponent, and non-isothermal flows in fractured-porous media.

To account for the simulation of the TEM data acquisition at predefined calibration times during the fluid injection process, a secondary forward modeling operator is coupled to the flow and transport simulator. We call it secondary, because the physical processes that are related to the TEM survey simulation are controlled by the (primary) physical system describing the fluid injection. In other words, the flow state within the reservoir at a given (flow) time t after injection begin controls the evolution of electrical properties, the latter being the forward modeling input to the TEM simulator.

Our inversion driver is based on iTOUGH2, an inverse-modeling implementation for TOUGH2 which contains additional tools for parameter sensitivity and uncertainty analysis [20]. For parameter estimation of TOUGH2 input (forward modeling) parameters, iTOUGH2 offers, among others, the Levenberg-Marquardt (L-M) modification of the Gauss-Newton algorithm which we use here. We use a modified version of iTOUGH2, called MPiTOUGH2 [14]. MPiTOUGH2 couples the TOUGH2 flow simulation to a variety of modularized seismic and electromagnetic geophysical simulators, where the employed TEM module is based on a parallel finite-difference implementation [48,13]. MPiTOUGH2 uses the Message Passing Interface (MPI) for parallel calculation of sensitivities needed for the L-M optimization as well as for the parallel solution of all partial differential equation systems resulting from the coupled forward-modeling operators.

The L-M optimization involves minimizing the quadratic approximation of the regularized objective function

$$\Theta = \left(\mathbf{z}^{obs} - \mathbf{z}(\mathbf{m})\right)^T \mathbf{C}_{zz}^{-1} \left(\mathbf{z}^{obs} - \mathbf{z}(\mathbf{m})\right), \tag{1}$$

where

$$\mathbf{z}^{obs} = \begin{pmatrix} \mathbf{z}_h^{obs} \\ \mathbf{z}_g^{obs} \end{pmatrix}$$

is a vector of size $N = N_H + N_G$, combining N_H hydrological (flow-rate) and N_G geophysical (TEM) data given by their individual stacks $\mathbf{z}_h^{obs}$ and $\mathbf{z}_g^{obs}$, respectively. Further, $\mathbf{C}_{zz}$ is the a priori covariance matrix which is a diagonal $N \times N$ matrix containing the observation errors, $\mathbf{m}$ is the vector of M model parameters, and $\mathbf{z}(\mathbf{m})$ is the composite vector of forward-modeling responses. Eq. 1 can be augmented by an additional regularization term. However, our parametric inversion for predefined shape parameters of a 3D fracture continuum already represents a strongly regularized case. Thus, Eq. 1 uses no additional regularization term.

2.3 Hydrogeophysical inversion of flow and geophysical data

The fact that Eq. 1 involves a stacked data vector, $\mathbf{z}^{obs}$, combining hydrological and geophysical observations, renders the minimization a hydrogeophysical inverse problem. The hydrological literature discusses many hydrogeophysical inverse applications. For example, Hinnell et al. (2010) provide a detailed discussion and comparison between the coupled inversion scheme and its counterpart, the uncoupled scheme. Many references therein point to applications of both schemes.

Expressed in a simplified way, the uncoupled scheme involves (usually two) separate (or sequential) inversions, each one minimizing a system of the type of Eq. 1. The first one is essentially a conventional geophysical inversion, with the vector of geophysical observations $\mathbf{z}_g^{obs}$ as data input. Converting its output, typically a spatial map of geophysical properties at a given (flow) time t, to some form of hydrological proxy data $\tilde{\mathbf{z}}_h^{obs}$ at that time t precedes the subsequent inversion, now for hydrological (fluid-flow-controlling) properties. In this latter inversion, the data input would thus be the stacked vector

$$\mathbf{z}^{obs} = \begin{pmatrix} \mathbf{z}_h^{obs} \\ \tilde{\mathbf{z}}_h^{obs} \end{pmatrix}$$

of actual hydrological data ($\mathbf{z}_h^{obs}$) and the added proxy-data component ($\tilde{\mathbf{z}}_h^{obs}$).

The uncoupled workflow could be applied to our parametric type of inverse problem. To be most effective, this would require a parametric implementation of the TEM data inversion. An alternative would involve inverting the TEM data for electrical conductivity on a dense pixel-based parameter grid. However, given the generally ill-posed nature of over-parameterized inversions, the fracture's electrical conductivity image would likely be prone to inversion artifacts. Artifacts would manifest in erroneous entries of $\tilde{\mathbf{z}}_h^{obs}$, thus adversely affecting the subsequent hydrological inversion.

While the discussion about the advantages of coupled versus uncoupled inversion schemes is ongoing, e.g. [9], we do not pursue this question any further here and choose a coupled approach. Our choice is based on the fact that the parametric type of inversion estimates structural parameters together with permeability parameters, thus somewhat making the intermediate geophysical inversion step (if using an uncoupled scheme) redundant.

Generally, both uncoupled and coupled schemes integrate hydrological and geophysical data types in order to carry out the estimation of hydrological properties that control the dynamic nature of the fluid-injection process. This is different to conventional geophysical joint inverse problems that, for example, combine seismic and electrical data seeking to delineate geophysical property contrasts of static targets, e.g. [21]. We therefore want to dedicate the next section to explain in a more pedagogic manner how flow and TEM data are joined within our coupled inversion framework.

2.4 Coupled inversion illustrated

Hydrogeophysical inversion schemes essentially have the goal of estimating those forward-modeling input parameters that control fluid flow. Geophysical observations can aid the estimation because they are indirectly sensitive to either spatial or temporal changes in hydrological material properties and/or flow states. This sensitivity stems from the fact that most geophysical material properties, such as electrical resistivity or seismic velocity, can be cast into hydrological proxy variables. Hence, they can be regarded as functional combinations of multiple hydrological quantities, often combining both material properties (e.g., porosity, density) and state variables (e.g. solute/tracer concentration, water/gas saturation). For example, the bulk rock electrical resistivity ϱ is often calculated as a function

$$\varrho = \varrho(\Phi, S, \varrho_f), \tag{2}$$

combining the quantities porosity Φ, fluid saturation S, and fluid electrical resistivity ϱ_f, where in our case the latter depends on solute (brine) concentration, C, that is, ϱ_f=$\varrho_f(C)$. Note that all these input quantities to ϱ are pertinent to the primary physical system describing our fluid injection scenario.

Fig. 2 illustrates how Eq. 2 connects the physical (hydro) system, describing fluid injection and flow, to a physical system for modeling the TEM data acquisition. For this illustrative example, we simulate the injection of brine into a shallow freshwater aquifer taking place over 5 days. A constant horizontal pressure gradient drives the spread of the injected fluid (from left to right). Hydraulic permeability is the governing hydrological material property that defines preferential flow paths and thus the brine's spatial spread over time. The bottom panel in Fig. 2 depicts the underlying actual permeability model, also indicating a major preferential flow path along the model bottom.

In this example, the hydrological data component consists of daily brine concentration samples $z_{h1}, \cdots, z_{h5}$ measured at a monitoring well bottom. Surface TEM data acquired at t=3 days after injection start provides the geophysical data. For the latter, the hydrological state $C(t = 3\,\text{days})$ defines the bulk

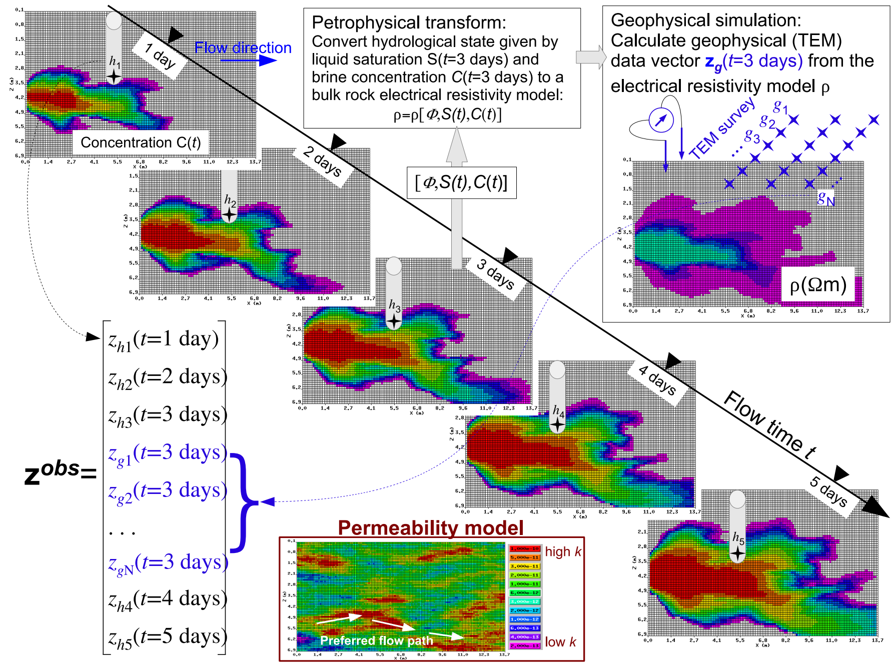

Fig. 2 Graphical illustration of the coupled hydrogeophysical inversion workflow. For mere illustration purposes, instead of a fracture case, the modeled scenario depicts a 2D model of a near-surface tracer injection. The underlying permeability model defines the spatial tracer plume evolution over the 5-day injection period and represents the model space of estimated parameters. The vector of observations $\mathbf{z}^{obs}$ combines N_H=5 hydrological data $z_{h1}, \cdots, z_{h5}$, measured daily at an observation well, with N_G geophysical surface TEM fields $z_{g1}, \cdots, z_{gN_G}$, the latter measured once at t=3 days. Input to this hydrogeophysical inversion workflow example comprises the stacked data vector $\mathbf{z}^{obs}$ and an initial (permeability) model guess.

electrical conductivity at t=3 days according to Eq. 2, thereby providing the model input to the TEM simulator. For simplicity, this case assumes the liquid saturation to be constant at S=1. Eq. 2 is often called a petrophysical transform, as it transforms hydrological variables to rock properties, which in our context are electrical properties.

Given the bulk rock electrical resistivity ϱ and a predefined transmitter-receiver configuration as input, the TEM simulation produces a vector of N_G electric field samples, $\mathbf{z}_g(\mathbf{m})$, as output. Typical TEM systems sample the transient decay of the electric field after source shutoff, where transient time window lengths of a few milliseconds up to a few seconds are common for surface applications. Assuming N_r receiver stations (N_r=18 in this example) and N_t electric field transient time samples per station (typically tens to a few hundred), the total number of TEM samples augmenting the combined data vector $\mathbf{z}^{obs}$ amounts to $N_G = N_r \times N_t$. The example also illustrates a commonality in hydrogeophysical applications with surface-based geophysical surveys.

Geophysical surface observations tend to be spatially dense, however, due to survey logistics, temporally sparse. The opposite often holds for hydrological well observations.

The main characteristic of a coupled hydrogeophysical inversion, as opposed to the aforementioned uncoupled scheme, is that the joint data vector $\mathbf{z}^{obs}$ undergoes one inversion sweep. Hence, there are only geophysical forward-modeling calls instead of the intermediate geophysical inversion. The coupled scheme illustrated through Fig. 2 inverts directly for the flow-process-defining parameters, which form some spatial distribution of permeability. If carried out in an iterative manner, every model-updating step would involve the forward-modeling of the 5-day fluid injection period coupled to the TEM simulation at t=3 days.

The following demonstration of the estimation of fracture-defining parameters will use this type of fully coupled workflow.

3 Coupled inversion scheme for fracture characterization

Two sets of inversions are carried out. The first set uses only hydrological (flow-rate) data, and the second set inverts both flow-rate and TEM data jointly using the coupled inversion workflow illustrated above. In the following, we first describe the hydrological and geophysical models and their data components separately before presenting the inversion results.

3.1 Hydrological model and data

The flow and transport simulator embedded within the coupled parameter estimation framework employs the TOUGH2 module EOS7 [39]. EOS7 treats gas (consisting of air and water vapor) and aqueous phase mixtures (consisting of water, brine, and dissolved air). We use this module in isothermal mode under conditions of full liquid saturation, i.e. no gas is present in the model.

For the proper representation of the ellipsoidal fracture zone illustrated in Fig. 1, we employ a 3D Cartesian TOUGH2 finite-volume mesh with a total of $78 \times 78 \times 29$=176,436 elements. Its node spacing is 1 m in the vicinity of the centered injection well with a gradual increase outwards. The flow model covers a volume of $413\,\mathrm{m} \times 413\,\mathrm{m} \times 285\,\mathrm{m}$. Fig. 3 shows the extent of the region where the electrical conductivity increases with respect to the background due to brine intrusion after the full injection period (70 min). Fig. 3b also delineates the volume of the flow model domain embedded into the geophysical model. For a view of the actual TOUGH2 flow modeling domain and its spatial mesh sampling, we refer to Fig. 4, where the actual model dimensions are shown by the red contours.

The brine spreads preferentially along the fracture zone. The permeability within that fracture continuum tampers off towards the edge of the ellipsoid,

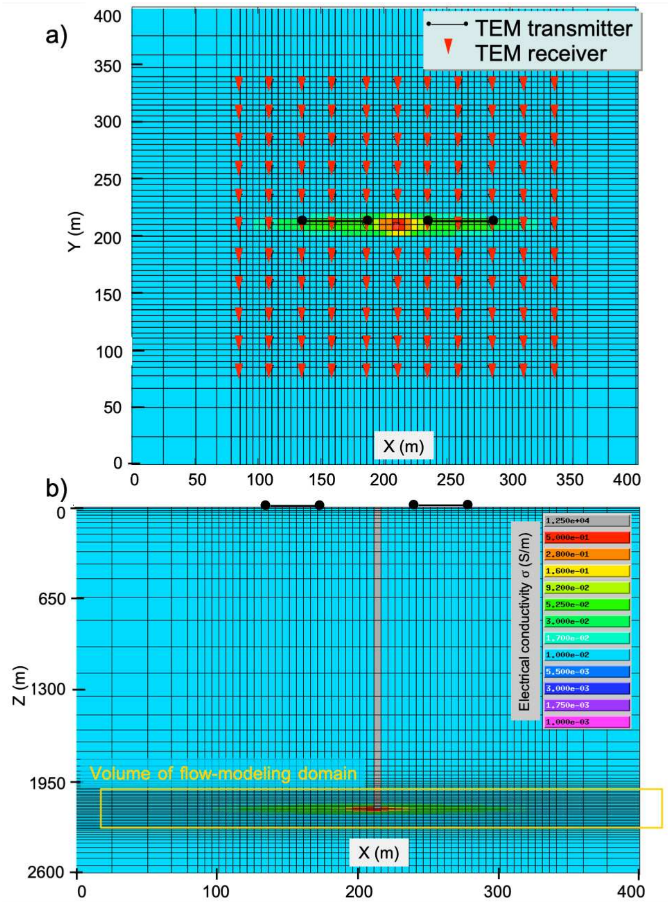

Fig. 3 TEM survey configuration and electrical conductivity anomaly due to brine injection into an existing fracture at a depth of z=2145 m. The upper figure shows a horizontal view of the TEM source and receiver surface setup, where the fracture anomaly is projected onto the surface.

representing reduced density and connectivity of the secondary fracture network away from the main hydrofracture. A spherical function is used to gradually reduce the permeability from the high values in the center of the ellipsoid to the low value of the background formation at the edge of the fracture zone. The injection rate declines with time as expected for any constant-pressure injection test in a composite system. Once the pressure perturbation reaches the edge of the fracture zone, the flow rates reach the transient behavior consistent with that of an unfractured, low-permeability formation, effectively stopping the further advancement of the brine plume. The flow rate data thus depend on the size of the fracture zone. However, it is obvious that the flow rates are not sensitive to the azimuth with which the fracture zone is embedded in the background formation. Additional, complementary data are therefore needed to identify both the hydrological properties of the stimulated fracture zone as well as its geometry.

The synthetic hydrological data set ($\mathbf{z}_h^{obs}$) considered here consists of flow rates in kg/s measured at the injection point. Injection takes place under a constant overpressure of 22.1 MPa (3205 psi) at the injection point. Logarithmic sampling of 50 data points starts at 1 s and ends at 4200 s (70 min). Synthetic, normally distributed noise with zero mean and a two percent standard deviation is added to the flow data.

3.2 TEM model and surface data configuration

Fig. 3a illustrates the geophysical survey configuration located at the surface (z=0 m) and centered over the fluid injection point (at z=2145 m). Electric fields are measured over an array of N_r=121 receiver locations, where only the E_x field component (parallel to x-axis) is considered. The E_x fields are sourced by two sequentially activated horizontal electric dipole transmitters of length 50 m that are galvanically coupled to the ground. Sequential source activation assumes no residual fields due to the first source before the second one is activated.

Measurement of the transient field decay at each receiver starts when the DC source current is shut off. The transient time window covers the time interval (in milliseconds) [10.0,215.4], where N_t=27 logarithmically spaced E_x fields are sampled per transient. The whole TEM data acquisition is carried out twice, first at the (flow) time t_1=35 min, then at t_2=70 min (after injection start). Given these two survey repetitions with two sources each, we have a total of $N_G = 2 \times 2 \times N_r \times N_t$=13,068 TEM-data points, which form our geophysical data vector $\mathbf{z}_g^{obs}$. As for the hydrological data, the TEM-data is also contaminated by synthetic, normally distributed noise with zero mean and a two percent standard deviation.

Fig. 3b also contrasts the vertical steel casing (gray column) against the background of ϱ=100 Ωm. Simulating actual casing dimensions, which is on the order of inches, would require a very small and thus computationally expensive finite-difference grid node distance. While this is feasible for standalone forward-modeling applications [15], it can be prohibitive for inverse modeling with many repeated forward-modeling instances. We thus employ a material averaging scheme that approximates the metallic electrical conductivity (10^6 S/m) into the finite-difference grid with only moderate refinement of the region around the casing [45]. The finite-difference grid has a minimum horizontal node distance of 5 m (upper Fig. 3), leading to a conductive pseudo-casing grid column with σ=1.25×10^4 S/m.

3.3 Petrophysical linkage between the hydrological and geophysical models

Coupling the TEM forward simulator to the flow and transport simulator involves a petrophysical linkage of the form of Eq. 2, as was also illustrated by

Fig. 2. Specifically, we use Archie's [5] law for full liquid saturation,

$$\varrho = \Phi^{1.67}\varrho_f(C), \tag{3}$$

where the quantity $\Phi^{1.67}$ is also known as the rock's formation factor. The porosity changes from Φ=0.107 within the fracture zone to Φ=0.033 within the background formation.

The fluid electrical conductivity $\sigma_f(C) = \frac{1}{\varrho_f(C)}$ is assumed to vary linearly with the concentration of an injected NaCl solution according to

$$\sigma_f = C\sigma_{inj} + (1-C)\sigma_{for}. \tag{4}$$

For this relationship, C=[0,1] becomes the injected (brine) fluid fraction which is assigned an electrical conductivity of σ_{inj}=35 S/m. This high fluid conductivity results from adopting our model's (constant) ambient reservoir temperature of T=63.5^o C together with a NaCl concentration of 150,000 ppm [40]. Eq. 4 further involves a background formation electrical conductivity of σ_{for}=3 S/m. This value resembles seawater properties, which is common in deep reservoirs.

To estimate the maximum electrical conductivity contrast resulting from Eqs. 3 and 4 in the vicinity of the injection point, we insert Φ=0.107, C=1, thus $\sigma_f = \sigma_{inj}$, yielding the background bulk rock electrical conductivity σ=0.84 S/m (ϱ=1.19 Ωm). Outside of the fracture zone, we have Φ=0.033, a minimum of C=0, thus $\sigma_f = \sigma_{for}$=3 S/m, which leads to σ=0.01 S/m (ϱ=100 Ωm).

4 Inversion results in comparison

We compare the results of two trial synthetic-data inversion realizations. The first one uses the flow-rate data as input, the second one uses the joint data set as input, combining flow-rate and TEM data. The inputs and outputs of the two trial inversion realizations are summarized quantitatively and qualitatively in Table 1 and Fig. 4, respectively. Both inversions employ identical sets of lower and upper parameter bounds and starting model guesses. Permeability parameters k use the SI unit m^2, where both actuals and their logarithms (log-base 10) are given.

Table 1 shows that the flow-rate data inversion overestimates the background permeability, which leads to an underestimated SRV. One expects a strong influence of the fracture zone's permeability on the flow rate measured at the injection point. Hence, both inversions properly estimate this parameter at the correct value of 10^{-12} m^2. All fracture parameters are correctly recovered by the joint inversion. Figs. 4 and 5 delineate the recovered (blue) fracture dimensions and orientation in comparison to the actual (red) geometry.

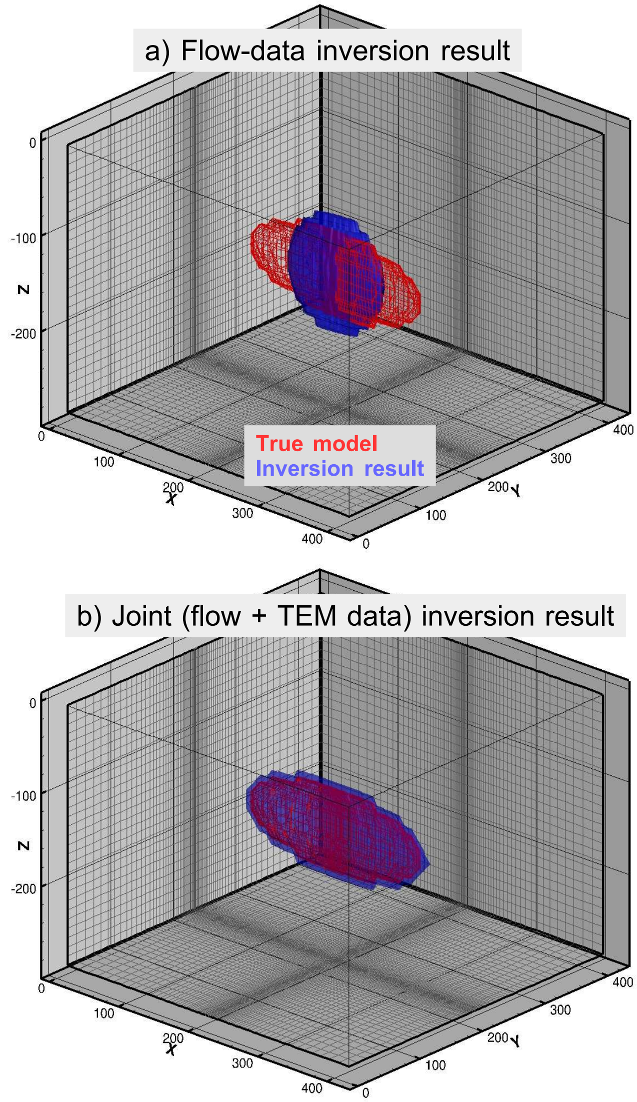

Fig. 4 Flow-rate data and joint (flow-rate and TEM data) inversion results in 3D view. The actual geometry of the fracture continuum is depicted by the red body. Mesh lines indicate the spatial discretization of the 3D TOUGH2 flow modeling domain.

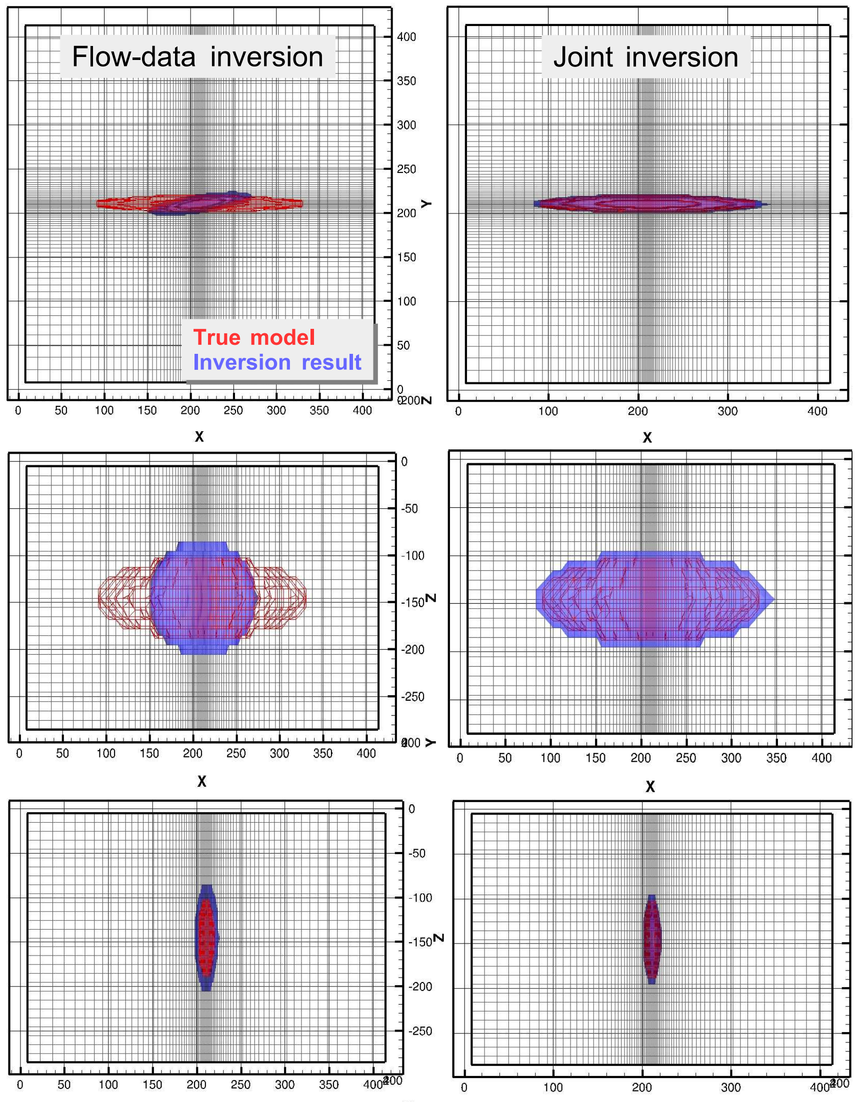

Fig. 5 Flow-rate data and joint (flow-rate and TEM data) inversion results. Shown are cross sections of the true (red) and estimated (blue) fracture bodies for the planes x-y (top), x-z (middle) and y-z (bottom). Mesh lines indicate the spatial discretization of the 3D TOUGH2 flow modeling domain.

4.1 Parameter sensitivities and uncertainties

To assess a measure of significance for the shown inversion results, we calculate uncertainties for each estimated parameter. Parameter uncertainties correspond to variances, which are the diagonal elements of the covariance matrix $\mathbf{C}_{pp}$ [10,19]:

$$\mathbf{C}_{pp} = \left(\mathbf{J}^T \mathbf{C}_{zz}^{-1} \mathbf{J}\right)^{-1}, \tag{5}$$

where $\mathbf{J}$ is the parameter sensitivity matrix (Jacobian) consisting of local sensitivity coefficients

$$S_{ij} = \frac{\partial z_i}{\partial p_j},\ i = 1, \cdots, N;\ j = 1, \cdots, 5.$$

For a given datum z_i, the sensitivity coefficient S_{ij} essentially quantifies its change due to a perturbation of an input (model) parameter p_j. In Eq. 5, $\mathbf{C}_{zz}$ is the $N \times N$ observation covariance matrix. In our case, $\mathbf{C}_{zz}$ is a diagonal matrix, where each diagonal element C_{ii} is the variance $\sigma_{z_i}^2$ calculated from the standard deviation σ_{z_i} assigned to the observation z_i. There exists an inverse proportionality between estimation uncertainty and the absolute size of the sensitivity coefficients S_{ij} [19].

Table 2 lists the uncertainties of the estimated parameters, which can be calculated from Eq. 5. The full covariance matrices without and with the inclusion of TEM data are shown in Tables 3 and 4, respectively. In these tables, the diagonal holds the variances, and the upper triangular matrix shows the covariances, which are easier to interpret if normalized [19]; the corresponding correlation coefficients are shown in the lower triangular matrix.

The comparison between the diagonal elements of the two matrices (summarized as estimation uncertainties in Table 2) clearly demonstrates the value of jointly inverting complementary data sets. While flow-rate data by themselves accurately identify the permeabilities, they do not contain sufficient independent information to determine the geometrical parameters (azimuth and extent) of the stimulated fracture zone. The high estimation uncertainties are a result of strong correlations among some of the geometrical parameters. For example, a correlation coefficient close to -1 indicates that a similar flow-rate response would result from increasing the fracture X-extent while decreasing the Z-extent. The very high uncertainty of the azimuth is mainly a result of the lack of sensitivity in the flow-rate data with respect to fracture orientation.

By adding TEM data, the information content of the joint data set is greatly increased, as would also be revealed by composite sensitivity measures [19]. Moreover, correlations among the parameters are reduced, in principle reducing the negative impact of an uncertain parameter on the estimation of another parameter. These comparisons indicate that the remote-sensing TEM data has the capacity to complement and enhance the information content of the flow-rate measurements without any in-situ interference with the hydraulic fracturing process.

Table 2 Parameter estimation uncertainties. Permeability uncertainties correspond to their log-base-10 transforms used in the inversion. Note that the uncertainties correspond to the square root of the diagonal elements of their covariance matrix (Tables 3 and 4).

Parameter type	Flow-rate inversion	Flow-rate and TEM inversion
Permeability rock matrix, $\log_{10}(k)$ (m^2)	2.1E-01	1.1E-01
Permeability fracture continuum, $\log_{10}(k)$ (m^2)	1.5E-03	9.5E-04
X-extent fracture continuum (m)	7.4E+01	8.2E+00
Z-extent fracture continuum (m)	7.4E+01	8.4E-01
Azimuth angle fracture continuum (deg)	2.1E+02	2.4E+00

Table 3 Flow-rate inversion: Covariance matrix (lower and diagonal) and correlation matrix (upper) of estimated parameters.

	Rock matrix k	Fracture k	X-extent	Z-extent	Azimuth
Rock matrix k	0.440E-01	0.594E+00	-0.879E+00	0.854E+00	0.323E+00
Fracture k	0.190E-03	0.233E-05	-0.385E+00	0.353E+00	-0.036E+00
X-extent	-0.136E+02	-0.435E-01	0.547E+04	-0.999E+00	-0.714E+00
Z-extent	0.132E+02	0.397E-01	-0.544E+04	0.543E+04	0.741E+00
Azimuth	0.145E+02	-0.117E-01	-0.113E+05	0.117E+05	0.461E+05

Table 4 Flow-rate and TEM joint inversion: Covariance matrix (lower and diagonal) and correlation matrix (upper) of estimated parameters.

	Rock matrix k	Fracture k	X-extent	Z-extent	Azimuth
Rock matrix k	0.011E+00	-0.506E+00	-0.652E+00	0.509E+00	-0.795E+00
Fracture k	-0.515E-04	0.914E-06	0.433E+00	-0.412E+00	0.285E+00
X-extent	-0.571E+00	0.341E-02	0.679E+02	-0.983E+00	0.085E+00
Z-extent	0.456E-01	-0.332E-03	-0.682E+01	0.710E+00	0.086E+00
Azimuth	-0.205E+00	0.662E-03	0.169E+01	0.176E+00	0.589E+01

Table 5 Initial and final RMS values calculated for both inversions. RMS values involve 50 flow-rate samples and 13,068 TEM-data points.

	Flow-rate data fit		TEM-data fit	
	Initial RMS	Final RMS	Initial RMS	Final RMS
Flow-rate inversion	779.05	1.59	-	-
Joint inversion	779.05	1.09	382.00	1.51

4.2 Data fits exemplified

Finally, a visual inspection of the achieved data fits lets us assess the performance of the two inversions in a qualitative manner. Fig. 6 compares the flow-rate data inversion result, showing observed (synthetic) data against those calculated from the initial (gray) and estimated final (blue) model parameters (parameter values are listed in Table 1). The high initial guess for the permeability of the fracture continuum accounts for an overestimated flow rate by an order of magnitude. Nevertheless, an exact match is achieved after 12 inversion iterations. Corresponding RMS values for the shown fits are given in Table 5. The goodness of fit, despite a grossly underestimated SRV, also is an indicator for the the flow rate's low degree of sensitivity with respect to resolving the fracture zone's geometrical attributes.

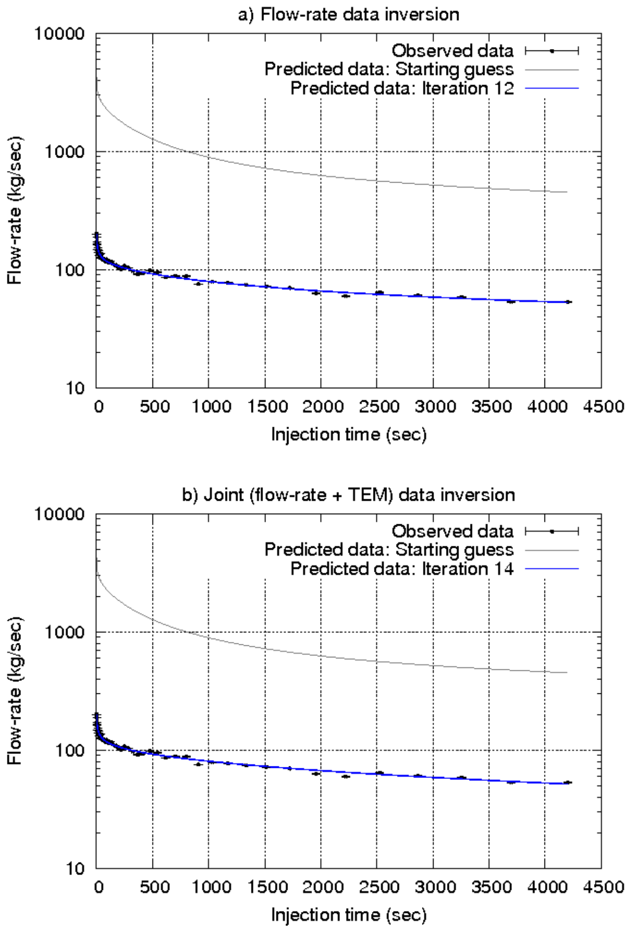

Fig. 6 Observed (synthetic) flow-rate data and data predictions calculated from initial (gray) and final (blue, after 12 inversion iterations) model guesses. Inversion results are shown for (a) hydrological (flow-rate data only) and (b) joint inversions.

Fig. 7 exemplifies one transient calculated from the joint (flow-rate and TEM-data) inversion result for a selected transmitter-receiver pair shown in blue in the TEM survey subplot. This transient exhibits a typical feature of TEM data, that is, the sign reversal of the electric field shortly before 0.1 s (measured after transmitter shutoff). Data points in the vicinity of such reversals usually need to be down-weighted in order to avoid their excessive influence on the minimization of Eq. 1. The joint inversion achieves a perfect match of the transient, which is also quantified by Table 5. It compares the initial and final RMS calculated for all 13,068 TEM-data points.

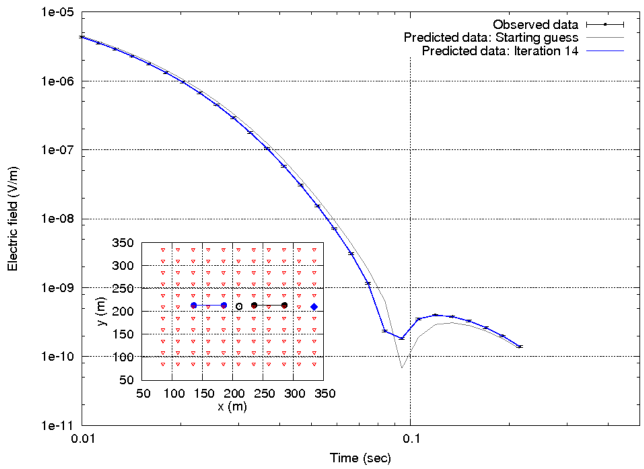

Fig. 7 Observed (synthetic) TEM (electric) field predictions calculated from initial (gray) and final (blue, after 14 inversion iterations) model guesses. The exemplified transient is calculated from the transmitter-receiver pair highlighted in blue in the station subplot. The TEM survey setup is also shown by Fig. 3. Absolute electric fields are plotted, showing the sign reversal around 0.1 s as a minimum.

5 Conclusions

This proof-of-concept has demonstrated the potential value of geophysical EM data for the characterization of hydraulically fractured reservoirs. Hydrogeophysical parameter estimation applications, whether they involve uncoupled or coupled approaches, have shown to benefit from the typically large spatial coverage and thus geometrical information of geophysical methods, e.g. [44].

Our article has the primary purpose of providing a proof-of-concept, extending already proven fracture-monitoring capabilities of the TEM method [28] towards imaging of fracture geometries. Along the way, we also laid out the inversion concepts of our coupled hydrogeophysical framework in some explanatory manner, because multi-physics imaging problems over fractures present a new and interdisciplinary challenge to the community.

The surface-based TEM method is suitable for large penetration depths; hence, it can complement hydraulic in-situ measurements of flow rates and may also provide an addendum to seismic data. With sufficient reservoir a priori data, the sensitivity to fluid property changes may also make TEM an economically attractive alternative to in-situ measurements as it allows for operational independence away from the injection well.

Under the condition that injected proppants with electrically contrasting properties fill the fracture periphery, EM data can provide a valid alternative to MEQ surveys in terms of providing geometrical information and SRV estimates. Theoretically, the TEM method has shown to yield data sensitivities that are needed for reliable estimates of SRV and fracture orientation. Nevertheless, for deep reservoirs, it is certainly beneficial to amplify the TEM source signal at the target depth by placing the surface transmitter in the vicinity of steel-cased wells, thus using the vertical current-channeling due to the metallic casing.

While our studies only consider a petrophysical link to the bulk rock ionic electrical conductivity, the sensitivity of EM methods can be increased by enhancing other than conductive (like capacitive or ferromagnetic) EM properties of injected fluids [7]. However, the upside of being sensitive to, for example, capacitive properties comes along with the necessity of properly simulating their footprint within numerical multi-physics modeling frameworks. Utilizing the induced-polarization effect, tracers with capacitive constituents may help a more precise pathway mapping of injected fluids in fracture zones. Both the presence of such tracers or a polarizable host rock would necessitate petrophysical links with complex, that is, having real and imaginary components, conductivity and complex permittivity properties.

With heterogeneity of rocks across field scales, the proper parameterization of petrophysical mapping functions that reflect all EM property dependencies may require ample laboratory data on drilled cores [33]. This may also become important in the presence of electrical formation anisotropy. Here, we only considered an isotropic model, because formation anisotropy, while important if field data contains its footprint, may only have a second-order impact on the detection sensitivities deduced here. The latter is an expectation requiring an upholding follow-up study. In the case of insufficient rock samples, one can alternatively include petrophysical parameters in the inversion process, e.g. [47]. In any case, the presence of formation anisotropy, as well as polarizable media, are most likely to require preceding standalone EM-data inversions in order to establish adequate background models for unbiased field-data inversions.

The diffusive nature of the TEM method and its resolution loss with depth somewhat forgives the approximation of complex fracture networks by a continuum, further justifying the use of a 3D parametric inversion approach. This assumes that the main objective does not go beyond the estimation of bulk quantities such as SRV or major fracture extent and orientation. Nevertheless, even with the aim of only a first-order geometrical identification, a next reasonable step towards fitness for real-world applications would involve accounting for porosity, i.e. storativity, in addition to (hydraulic) permeability. Another step along these lines is the modeling of horizontal casings, prevalent at hydraulic-fracturing sites. For this purpose, numerical EM modeling methods using OcTree meshes [23] have shown better local refinement abilities than finite-difference methods.

Acknowledgements Funding for this work was provided by Chevron Energy Technology Company. The addition of the TEM simulator module to the inversion framework was also supported by the U.S. Department of Energy, Office of Science, Office of Basic Energy Sciences, Chemical Sciences, Geosciences, and Biosciences Division under Contract DE-AC02-05CH11231. Development of the MPiTOUGH2 architecture was supported through a laboratory-directed research and development (LDRD) grant by Lawrence Berkeley Nat'l Lab for MC.

References

1. Abass, H.H.: Oriented perforating helps ensure successful well completions. Oil and Gas Journal, 93, 80-85 (1995)
2. Ahmadian, M., LaBrecque, D., Liu, Q.H., Slack, W., Brigham, R., Fang, Y., Banks, K., Hu. Y., Wang, D.: Zhang, R.: Demonstration of proof of concept of electromagnetic geophysical methods for high resolution illumination of induced fracture networks. Society of Petroleum Engineers, doi:10.2118/189858-MS (2018)
3. Al Hagrey, S.A.: Electric study of fracture anisotropy at Falkenberg, Germany. Geophysics, 59, 881-888 (1994)
4. Al-shehri, A., Ellis, E., Servin, J., Kosynkin, D., Kanj, M., Schmidt, H.:. Illuminating the reservoir: Magnetic NanoMappers. SPE Middle East Oil and Gas Show and Conference Proceedings, 3, 10 p. (2013)
5. Archie, G.E.: The electrical resistivity log as an aid in determining some reservoir characteristics. Trans. Am. Inst. Min. Metall. Petrol. Eng., 146, 54-62 (1942)
6. Becker, M.W., Tsoflias, G.P.: Comparing fluxaveraged and resident concentration in a fractured bedrock using ground penetrating radar, Water Resour. Res., 46, W09518 (2010)
7. Bicerano, J.: Proppants coated by piezoelectric or magnetostrictive materials, or by combinations thereof. US Patent No. 8,006,755 B2 (2011)
8. Burtman, V., Fu, H., Zhdanov, M.S.: Experimental study of induced polarization effect in unconventional reservoir rock. Geomaterials, 4, 117-128 (2014)
9. Camporese, M., Cassiani, G., Deiana, R., Salandin, P., Binley, A.: Coupled and uncoupled hydrogeophysical inversions using ensemble Kalman filter assimilation of ERT-monitored tracer test data. Wat. Resour. Res., 51, 3277-3291 (2015)
10. Carrera, J., Neuman, S.P.: Estimation of aquifer parameters under transient and steady state conditions: 1. Maximum likelihood method incorporating prior information. Water Resour. Res., 22(2), 199-210 (1986)
11. Chen, J., Hubbard, S., Peterson, J., Williams, K., Fienen, M., Jardine, P., and Watson, D.: Development of a joint hydrogeophysical inversion approach and application to a contaminated fractured aquifer. Water Resour. Res., 42, W06425 (2006)
12. Chichinina, T., Sabinin, V., Ronquillo-Jarillo, G.: QVOA analysis: P-wave attenuation anisotropy for fracture characterization. Geophysics, 71, C37C48 (2006)
13. Commer, M., Newman, G.A.: A parallel finite-difference approach for 3D transient electromagnetic modeling with galvanic sources. Geophysics, 69, 11921202 (2004)
14. Commer, M., Kowalsky., M.B., Doetsch, J., Newman, G.A., Finsterle, S.: MPiTOUGH2: A parallel parameter estimation framework for hydrological and hydrogeophysical applications. Computers and Geosciences, 65, 127-135 (2014)
15. Commer, M., Hoversten, G.M., Um, E.S.: Transient-electromagnetic finite-difference time-domain earth modeling over steel infrastructure. Geophysics, 80, E147-E162 (2015)
16. Day-Lewis, F.D., Slater, L.D., Robinson, J., Johnson, C.D., Terry, N., Werkema, D.: An overview of geophysical technologies appropriate for characterization and monitoring at fractured-rock sites, Journal of Environmental Management, 204, 709-720 (2017)
17. Dorn, C., Linde, N., Le Borgne, T., Bour, O., Klepikova, M.: Inferring transport characteristics in a fractured rock aquifer by combining singlehole groundpenetrating radar reflection monitoring and tracer test data. Water Resour. Res., 48, W11521 (2012)
18. Fang, X., Fehler, M.C., Zhu, Z., Zheng, Y., Burns, D.R.: Reservoir fracture characterization from seismic scattered waves. Geophys. J. Int., 196(1), 481-492 (2014)
19. Finsterle, S.: Practical notes on local data-worth analysis. Wat. Resour. Res., 51, 9904-9924 (2015)
20. Finsterle, S., Commer, M., Edmiston, J., Jung, Y., Kowalsky, M.B., Pau, G.S.H., Wainwright, H., Zhang, Y.: iTOUGH2: A simulation-optimization framework for analyzing multiphysics subsurface systems. Computers and Geosciences, 108, 8-20 (2017)
21. Gallardo, L.A., Meju, M.: Characterization of heterogeneous near-surface materials by joint 2D inversion of dc resistivity and seismic data. Geophys. Res. Lett., 30, 1658-1661 (2003).
22. Gunagqing, Z., Mian, C.: Complex fracture shapes in hydraulic fracturing with orientated perforations. Petrol. Explor. Develop., 36, 103-107 (2009)

23. Haber, E., Schwarzbach, C., Shekhtman, R.: Modeling electromagnetic fields in the presence of casing. SEG Technical Program Expanded Abstracts, 959-964 (2016)
24. Heagy, L.J., Oldenburg, D.W., Chen, J.: Where does the proppant go? Examining the application of electromagnetic methods for hydraulic fracture characterization. GeoConvention 2014, CSEG, Search and Discovery, Article 90224 (2014)
25. Hibbs, A.D.: Evaluation of deep subsurface resistivity imaging for hydrofracture monitoring. US DOE, National Energy Technology Laboratory, 5th Quart. Progr. Rep. Proj. No.: DE-FE0013902 (2015)
26. Hickey, M.S., Treviño, S., Everett, M.E.: Detection and characterization of the injection of hydraulic fracturing fluid using ground-based controlled-source electromagnetics. SEG Technical Program Expanded Abstracts (2015)
27. Hinnell, A.C., Ferré, T.P.A., Vrugt, J.A., Huisman, J.A., Moysey, S., Rings, J., Kowalsky, M.B.: Improved extraction of hydrologic information from geophysical data through coupled hydrogeophysical inversion. Wat. Resour. Res., 46, W00D40 (2010)
28. Hoversten, G.M., Commer, M., Haber, E., Schwarzbach, C.: Hydro-frac monitoring using ground time-domain electromagnetics. Geophys. Prospect., 63, 1508-1526 (2015)
29. Johnston, D.H. (ed.): Methods and applications in reservoir geophysics. Society of Exploration Geophysicists, Tulsa Oklahoma (2010)
30. Kang, P.K., Zheng, Y., Fang, X., Wojcik, R., McLaughlin, D., Brown, S., Fehler, M.C., Burns, D.R., Juanes, R.: Sequential approach to joint flow-seismic inversion for improved characterization of fractured media. Water Resour. Res., 52, 903-919 (2016)
31. Klein, J.D., Martin, P.R., Allen, D.F.: Petrophysics of electrically anisotropic reservoirs. The Log Analyst, 38, 25-36 (1997)
32. LaBrecque, D., Brigham, R., Denison, J., Murdoch, L., Slack, W., Liu, Q.H., Fang, Y., Dai, J., Hu, Y., Yu, Z., Kleinhammes, A., Doyle, P., Wu, Y., Ahmadian, M.: Remote imaging of proppants in hydraulic fracture networks using electromagnetic methods: results of small-scale field experiments. Society of Petroleum Engineers, doi:10.2118/179170-MS (2016)
33. Lesmes, D.P., Friedman, S.P.: Relationships between the electrical and hydrogeological properties of rocks and soils. In: Rubin, Y., Hubbard S.S. (eds) Hydrogeophysics. Water Science and Technology Library, vol 50. Springer, Dordrecht (2005)
34. Liang, F., Sayed, M., Al-Muntasheri, G.A., Chang, F.F., Li, L.: A comprehensive review on proppant technologies. Petroleum, 2, 26-39 (2016)
35. Maxwell, S.C., Urbancic, T.I.: The role of passive microseismic monitoring in the instrumented oil field. Lead. Edge 20(6), 636-639 (2001)
36. Nabighian, M.N., Macnae, J.C.: Time domain electromagnetic prospecting methods, in M.N. Nabighian, ed., Electromagnetic methods in applied geophysics - Applications, Vol. 2, SEG, 427-520 (1991)
37. Palisch, T., Al-Tailji, W., Bartel, L., Cannan, C., Zhang, J., Czapski, M., Lynch, K.: Far-field proppant detection using electromagnetic methods - latest field results. Paper number SPE-184880-MS, Soc. Petrol. Eng. Hydraulic Fracturing Technology Conf. and Exhib., The Woodlands, TX (2017)
38. Pardo, D., Torres-Verdin, C.: Sensitivity analysis for the appraisal of hydrofractures in horizontal wells with borehole resistivity measurements. Geophysics, 78, D209-D222 (2013)
39. Pruess, K., Oldenburg, C., Moridis, G.: TOUGH2 Users Guide, Version 2.1. Rep. LBNL-43134, Lawrence Berkeley Natl. Lab., Berkeley Calif. (2012)
40. Schlumberger Wireline and Testing: Schlumberger log interpretation charts (2009 Ed.), 310 p. Schlumberger, Sugar Land, Texas (2009)
41. Shakas, A., Linde, N., Baron, L., Bochet, O., Bour, O., and Le Borgne, T.: Hydrogeophysical characterization of transport processes in fractured rock by combining pushpull and singlehole ground penetrating radar experiments. Water Resour. Res., 52, 938-953 (2016)
42. Shen, J., Su, B., Guo, N.: Anisotropic characteristics of electrical responses of fractured reservoir with multiple sets of fractures. Petroleum Science, 6, 127-138 (2009)
43. Spies, B.R.: Depth of investigation in electromagnetic sounding methods. Geophysics, 54, 872-888 (1989)
44. Steklova, K., Haber, E.: Joint hydrogeophysical inversion: state estimation for seawater intrusion models in 3D. Comput. Geosci., 21, 75-94 (2017)

45. Um, E.S., Commer, M., Newman, G.A., Hoversten, G.M.: Finite element modelling of transient electromagnetic fields near steel-cased wells. Geophys. J. Int., 202(2), 901-913 (2015)
46. Vereecken, H., Binley, A., Cassiani, G., Revil, A., Titov, K.: Applied hydrogeophysics, NATO Science Series 71, Springer, Netherlands (2006)
47. Vilhelmsen, T. N., Behroozmand, A.A., Christensen, S., Nielsen, T.H.: Joint inversion of aquifer test, MRS, and TEM data. Water Resour. Res., 50, 3956-3975 (2014)
48. Wang, T., Hohmann, G.W.: A finitedifference time-domain solution for three-dimensional electromagnetic modeling: Geophysics, 58, 797-809 (1993)
49. Wilt, M., Alumbaugh, D.L.: Oil field reservoir characterization and monitoring using electromagnetic geophysical techniques. J. Petrol. Sci. Eng., 39, 85-97 (2003)
50. Yan, L., Chen, X., Tang, H., Xie, X., Zhou, L., Hu, W., Wang, Z.: Continuous TDEM for monitoring shale hydraulic fracturing. Appl. Geophys., 15, 26-34 (2018)
51. Wu, Y.-S. (ed.): Hydraulic fracture modeling, p. 543. Gulf Professional Publishing, Cambridge MA (2018)